Journal of Magnetic Resonance **156,** 258–261 (2002)
doi:10.1006/jmre.2002.2564

A Two-Dimensional Artifact from Asynchronous Decoupling

Hugo van Ingen, Geerten W. Vuister, and Marco Tessari[1]

Department of Biophysical Chemistry, NSRIM Center, University of Nijmegen, Toernooiveld 1, 6525 ED Nijmegen, The Netherlands

Received December 21, 2001; revised May 10, 2002

Many heteronuclear NMR experiments employ decoupling to collapse the heteronuclear multiplet, using decoupling schemes with a periodic phase modulation like WALTZ, MLEV, or GARP. Because of the periodic nature of these schemes, cycling sidebands are generated, whose intensity can be strongly reduced by decoupling asynchronously. We show that the most common implementation of asynchronous decoupling on modern spectrometers is such that the cycling sidebands are subjected to a periodic modulation. For multidimensional experiments, this results in ridges that can seriously compromise the quality of the spectrum. Based on our model, the artifact in a 2D $\{^1H\}$–^{15}N NOE equilibrium experiment is simulated and it is shown that the artifact can be prevented by using synchronous decoupling.

Key Words: **asynchronous decoupling; heteronuclear NOE; cycling sidebands; broadband decoupling; WALTZ.**

INTRODUCTION

Heteronuclear NMR experiments on biomolecular systems often require decoupling during acquisition to collapse the multiplet resulting from scalar coupled spins. Heteronuclear decoupling removes the effects of the scalar coupling and typically yields both a higher resolution and sensitivity. Phase modulated schemes like WALTZ, MLEV, and GARP (*1–3*) have greatly improved the quality of decoupling, allowing for efficient removal of the scalar coupling at relatively low power, while maintaining a large decoupling bandwidth. The drawback of these sequences is that they generate so-called *cycling sidebands* because data acquisition occurs at intervals other than the refocusing of the *J*-coupling (*4–6*). Cycling sidebands are undesirable because they can overlap with signals of interest and reduce the intensity of the parent signal (*6, 7*). The intensity of these sidebands can be strongly attenuated by decoupling asynchronously in combination with time-averaging (*4–6*).

In the asynchronous mode, decoupling starts from a different point in the phase modulation pattern of each acquisition, resulting in a (partial) randomization of the phase of the sidebands (*5, 6*). In contrast, in the synchronous mode, decoupling starts each time from the beginning of the modulation sequence, resulting in identical sidebands. For example, asynchronization can be achieved by changing the decoupler pulse length (*8*) or by cyclically permuting an element of the phase modulation sequence (*5*). The most commonly used method on modern spectrometers is depicted in Fig. 1, which we refer to as the "jump–resume" implementation.[2] In this implementation decoupling is stopped at the end of acquisition, potentially in the middle of an element of the phase modulation scheme. In the successive scan, at the start of acquisition, decoupling is resumed from the following element in the decoupling sequence.

Here we show that, for a multidimensional experiment, this implementation of asynchronous decoupling introduces a periodic modulation of the cycling sidebands, resulting in a multidimensional artifact with defined frequencies in the indirect dimension. As an example, Fig. 2a shows the spectrum of a 2D heteronuclear NOE experiment employing asynchronous WALTZ-16 decoupling. The quality of the spectrum is seriously compromised by several horizontal ridges, making it impossible to determine the peak intensity for a number of residues. We show that these ridges, while they appear to be modulated in the indirect dimension, are actually generated by the cycling sidebands in the direct dimension. Hence, we call this a two-dimensional artifact.

THEORY

Ideally, asynchronous decoupling would involve complete randomization of the decoupling starting point to achieve optimal suppression of sidebands, since their phase and intensity depend on the point in the modulation pattern at which decoupling is started (*5*). However, using a "jump–resume" implementation of asynchronous decoupling, the starting point is not randomized. Although from scan to scan decoupling starts from different elements in the sequence, a periodicity is generated equal at most to the number of elements in the phase modulation sequence. The number of elements is different for different decoupling schemes and depends on their specific implementation.

Since our experiments employed WALTZ decoupling, we shall now extend our arguments for this case, but similar

[1] To whom correspondence should be addressed. E-mail: marco@nmr.kun.nl.

[2] We have observed this artifact on different types of spectrometers of different manufacturers. Personal communication with the technical departments of both Bruker A. G. and Varian Inc. confirmed the "jump–resume" implementation of asynchronous decoupling.

1090-7807/02 $35.00

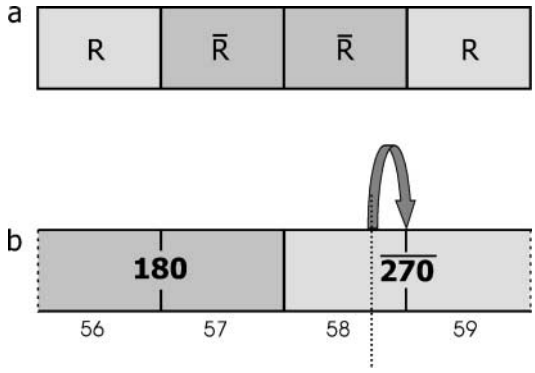

FIG. 1. (a) Schematic representation of the WALTZ-16 supercycle (*1*), where R is given by 270−$\overline{360}$−180−$\overline{270}$−90−$\overline{180}$−360−$\overline{180}$−270, the numbers refer to the pulse rotation angles, and the overbars indicate phase-inverted pulses. The total length of the supercycle is 96 times the 90°-decoupler pulse length. (b) Implementation of "jump–resume" asynchronous decoupling. The boxes represent the 90°-elements of the modulation pattern, the numbers in the boxes refer to the elements of R, and the numbers below the boxes indicate the index of that 90°-element. When acquisition is stopped somewhere in a 90°-element (indicated by the dotted line), decoupling resumes from the next 90°-element at the following acquisition; this "jump" is indicated by the arrow. This figure depicts the situation when decoupling started at element 1 in the previous scan, using Eq. [2] with an acquisition time equal to 0.0768 s and a 90° decoupling pulse of 222 μs.

reasoning holds for other decoupling schemes as well. Figure 1 schematically depicts the implementation of WALTZ-16 decoupling (*1*). Although its bandwidth is relatively limited, WALTZ-16 generates few sidebands, making it an appropriate choice for ^{15}N-decoupling. The implementation of WALTZ-16 decomposes the modulation sequence, or supercycle, in 96 elements, each of the duration of a 90°-pulse at decoupling power and each with a certain phase (cf. Fig. 1b). Therefore, decoupling starts from the same element again after at most 96 scans, generating identical sidebands in scan 1 and 97, 2 and 98, and so on. The exact period can be calculated, considering that the starting element is shifted regularly from scan to scan by a fixed number of 90°-elements, solely depending on the durations of the acquisition time and the WALTZ-16 supercycle. This shift can be expressed as a fraction of a supercycle, as indicated by the expressions

$$shift = \frac{n}{96}, \qquad [1]$$

where

$$n = \mathbf{int}\left(96 \times \mathbf{fract}\left(\frac{at}{W16}\right)\right) + 1 \qquad [2]$$

and *at*, *W16* denote acquisition time and duration of the WALTZ-16 supercycle, respectively; **int**(x) returns the integer part of x, **fract**(x) returns the decimal part of x, and n is the number of 90°-elements by which the starting element is shifted each scan (cf. Fig. 1).

From Eq. [1] it can be deduced that, independent of *at* and *W16*, the shift is equal to an integer multiple of supercycles after at most 96 scans, but smaller periods can also be expected for some values of n. As a result, the sidebands are modulated periodically and consequently cancellation artifacts, resulting from pairwise subtraction of scans, will be modulated periodically too. According to the Fourier theorem, the cancellation artifact can then be described as a superposition of sinusoidal components oscillating at the fundamental frequency and its harmonics.

For a multidimensional experiment, the cycling sidebands and the cancellation artifact accumulated in every FID are modulated

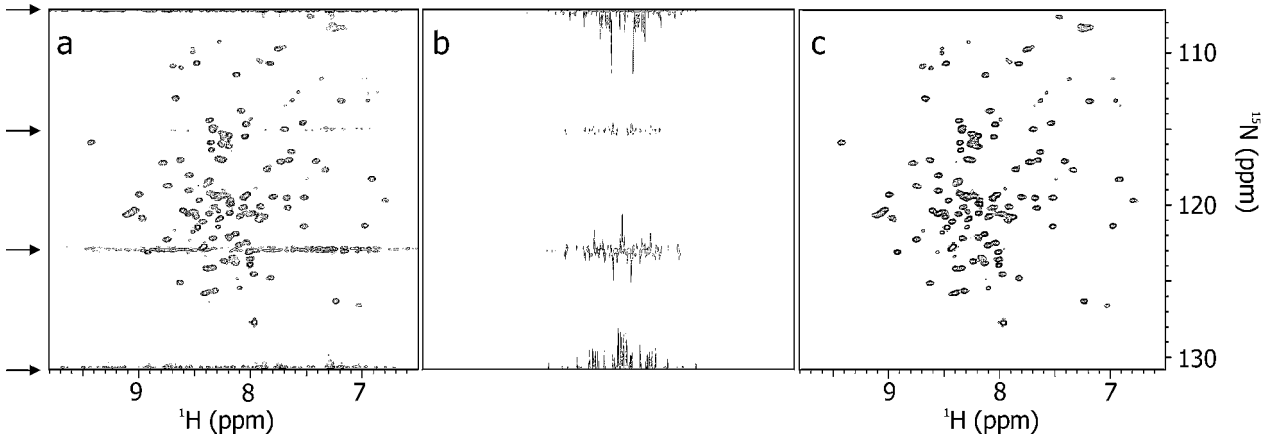

FIG. 2. (a) The {^{1}H}–^{15}N NOE equilibrium spectrum of the PAH2:MAD-SID24 complex using asynchronous WALTZ-16 decoupling with 1.12-kHz RF-field strength (90°-pulse of 222 μs). The arrows indicate the ridges. The sample was dissolved in an 95% H_2O/5% D_2O mixture, the pH was set to 6.3 using a phosphate buffer, and 50 mM of KCl as well as trace amounts of NaN_3 and protease inhibitor were added. Experimental parameters: acquisition time was set to 0.0768 s, the spectral width was 10000 Hz (t_2) × 1200 Hz (t_1), 32 scans were averaged per FID, and 120 complex points were recorded. (b) Simulated spectrum of an AX spin system with asynchronous WALTZ-16 decoupling, using the experimental parameters of (a). (c) Same as (a), but now with synchronous decoupling. All spectra were acquired on a Varian Unity Inova 500-MHz spectrometer. Spectra were processed using NMRPipe (*13*).

with a certain period of FIDs, depending on the number of scans per FID. The periodicity of this modulation results, after Fourier transformation, in horizontal ridges through the spectrum at a specific position in the indirect dimension given by the fundamental frequency and its harmonics.

RESULTS AND DISCUSSION

The heteronuclear $\{^1H\}$–^{15}N NOE experiment (cf. Fig. 3a) is an example of a multidimensional experiment which, due to its low sensitivity, may suffer from the artifact described above. Figure 2a shows the equilibrium spectrum of the $\{^1H\}$–^{15}N NOE experiment performed on a uniformly $^{13}C/^{15}N$-labeled 12.5-kDa protein studied in our laboratory. The artifact shown is common for any NOE equilibrium experiment run on a modern spectrometer using asynchronous decoupling and a pulse sequence relying on phase cycling to remove the equilibrium proton magnetization. Since the latter magnetization is 10 times larger than the signal originating from the nitrogen spins, the ridges generated by the cycling sidebands of the equilibrium proton signals are relatively large compared to the selected signals.

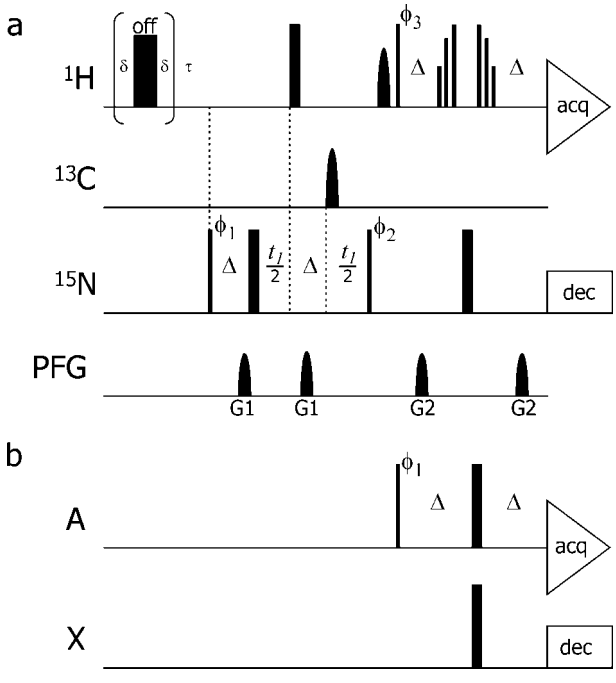

FIG. 3. (a) Pulse sequence of the $\{^1H\}$–^{15}N NOE experiment. The saturation pulse train composed of 135°-pulses is given off-resonance to record the equilibrium spectrum. The delay Δ is set to $\frac{1}{4}J_{N-H}$. The following phase cycle is used to cancel the equilibrium proton magnetization and to select the magnetization originating from the nitrogen spins: $\phi_1 = x, -x; \phi_2 = y, y, -y, -y; \phi_3 = -x; \Phi_{rec} = x, -x, -x, x$. States-TPPI was implemented on ϕ_1 (*9*). The water was put along the z-axis using a half-gauss-shaped water flip-back pulse. The residual water in the x,y-plane was suppressed by 3-9-19 WATERGATE pulses (*14*) in the reverse INEPT-block. Gradient strengths were 24 and 15 Gauss/cm for G1 and G2, respectively. (b) Pulse sequence used in the simulation program to calculate Fig. 2b. Spin X is decoupled asynchronously using WALTZ-16 modulation with a "jump–resume" implementation. The phase cycle $\phi_1 = x, x; \Phi_{rec} = x, -x$ cancels the equilibrium magnetization of spin A. The delay Δ is set to $\frac{1}{4}J_{A-X}$.

The position of the ridges can be rationalized using the equation

$$ns_{cp} \times shift = shift_{cp}, \quad [3]$$

where ns_{cp} is the number of scans per complex point, *shift* is given by Eq. [1], and $shift_{cp}$ is the shift of the starting element per complex point.

Substitution of the experimental settings for *at* and *W16* (76.8 ms and 96*222 μs, respectively, cf. Fig. 2) in Eq. [2] shows that the starting point of decoupling is shifted by 58 90°-elements for each transient (n), resulting, after substitution in Eq. [1], in a *shift* per scan equal to 58/96 supercycle. Because 32 transients were averaged per FID and States-TPPI quadrature detection (*9*) was used, ns_{cp} is equal to 64, resulting, after substitution in Eq. [3], in a shift per complex point equal to $38\frac{2}{3}$. As a consequence, after three complex points, the shift is equal to an integer number of supercycles. Thus, the cancellation artifact is modulated with a period of three complex points, resulting in two ridges at a frequency of ± one-third of the spectral width in the indirect dimension.

Figure 2a shows two ridges along the edges of the spectrum and two ridges dividing the total spectrum into three equal parts, as indicated by the arrows. Since States-TPPI was used to shift any signal not modulating in t_1 by half the sweep width, the zero frequency reference for the artifact is at the border of the spectrum. In perfect agreement with the theoretical period of three complex points, two ridges appear at a frequency of ± one-third of the sweep width of the indirect dimension (i.e., ± one-sixth of the sweep width relative to the center of the spectrum). The ridges at the border stem from the zero-frequency component of the artifact and/or aliased harmonics.

To simulate this two-dimensional artifact, a program was written in OCTAVE (*10*), which simulates the effect for an AX two-spin system. After generating $2\mathbf{A}_y\mathbf{X}_z$ antiphase coherence, spin X is subjected to asynchronous decoupling using a WALTZ-16 modulation scheme (cf. Fig. 3b). The evolution of the density matrix of this system is calculated numerically, taking Larmor precession, J-coupling, relaxation, and decoupling into account. The receiver phase is inverted every second scan, thus allowing complete focus on the cancellation artifact generated by the cycling sidebands of the main signal. This basic 1D-experiment was expanded into a 2D-experiment by repetitive evaluation using the experimental parameters of the actual $\{^1H\}$–^{15}N NOE experiment. The final calculated two-dimensional data matrix was then processed in an identical fashion as the experimental data.

The resulting spectrum displays ridges at positions identical to those observed in the experimental spectrum (cf. Fig. 2b). In addition, similar relative intensities are reproduced. Figure 2b also clearly shows the two-dimensionality of the artifact. A single signal generates many cycling sidebands appearing at the

decoupler cycling rate and its harmonics (*4*), and all are subjected to identical modulations, thus creating ridges parallel to the horizontal axis. While other studies describing artifacts from cycling sidebands in two dimensions (*11, 12*) have used decoupling in the indirect dimension, we show that the artifact introduced by asynchronous decoupling during t_2 is inherently two-dimensional.

Since the artifact is caused by the cycling sidebands of the large unwanted equilibrium proton signal, it can be prevented by decoupling synchronously. Each scan generates identical sidebands ensuring perfect subtraction of the unwanted signal. This is shown in Fig. 2c, which displays the $\{^1H\}$–^{15}N NOE experiment recorded with synchronous decoupling, but using otherwise identical experimental parameters as for Fig. 2a. As is immediately evident, the artifact has completely disappeared.

Alternatively, the artifact can be prevented by using a different implementation of asynchronous decoupling, ensuring a truly random starting element of the decoupling sequence. This would lead to the loss of the modulation of the cycling sidebands, resulting in a slight increase of t_1-noise, as confirmed by our simulations (data not shown).

CONCLUSION

We have shown that the "jump–resume" implementation of asynchronous decoupling results in a periodic modulation of the cycling sidebands. For a multidimensional experiment this results in ridges through the spectrum, as shown for the heteronuclear NOE equilibrium experiment. This artifact is multidimensional in nature, since the apparent frequencies along the indirect dimension actually stem from modulations in the direct dimension. Other phase-modulated decoupling schemes like GARP and MLEV have been shown to give rise to similar artifacts (data not shown).

The artifact presented here is a common problem for any insensitive experiment that relies on phase cycling to cancel a relatively large unwanted signal and uses asynchronous decoupling. Synchronous decoupling and a different implementation of asynchronous decoupling are possible solutions to this problem.

ACKNOWLEDGMENTS

We thank Professor Dr. C. W. Hilbers for his stimulating interest and Tine Walma for her constructive comments on the manuscript. Hugo van Ingen is supported by the Dutch Organization of Scientific Research, NWO.

REFERENCES

1. A. J. Shaka, J. Keeler, T. Frenkiel, and R. Freeman, An improved sequence for broadband decoupling: WALTZ-16, *J. Magn. Reson.* **52,** 335–338 (1983).
2. M. H. Levitt, R. Freeman, and T. Frenkiel, Broadband heteronuclear decoupling, *J. Magn. Reson.* **47,** 328–330 (1982).
3. A. J. Shaka, P. B. Barker, and R. Freeman, Computer-optimized decoupling scheme for wideband applications and low-level operation, *J. Magn. Reson.* **64,** 547–552 (1985).
4. R. Freeman, T. Frenkel, and M. H. Levitt, A simple "black-box" decoupler, *J. Magn. Reson.* **50,** 345–348 (1982).
5. A. J. Shaka, P. B. Barker, C. J. Bauer, and R. Freeman, Cycling sidebands in broadband decoupling, *J. Magn. Reson.* **67,** 396–401 (1986).
6. A. J. Shaka, J. Keeler, and R. Freeman, Evaluation of a new broadband decoupling sequence: WALTZ-16, *J. Magn. Reson.* **53,** 313–340 (1983).
7. E. Kupče, R. Freeman, G. Wider, and K. Wüthrich, Suppression of cycling sidebands using bi-level adiabatic decoupling, *J. Magn. Reson. Ser. A* **122,** 81–84 (1996).
8. R. W. Dijkstra, A method to suppress cycling sidebands in broadband decoupling, *J. Magn. Reson.* **82,** 347–351 (1989).
9. D. Marion, M. Ikura, R. Tschudin, and A. Bax, Rapid recording of 2D NMR spectra without phase cycling: Application to the study of hydrogen exchange in proteins, *J. Magn. Reson.* **85,** 393–399 (1989).
10. GNU Octave is a high-level language, primarily intended for numerical computation and is freely available from http://www.octave.org.
11. S. Zhang and D. G. Gorenstein, Synchronized adiabatic decoupling, *J. Magn. Reson.* **147,** 110–115 (2000).
12. E. Kupče and R. Freeman, A two-dimensional experiment that separated decoupling sidebands from the main peaks, *J. Magn. Reson.* **151,** 142–145 (2001).
13. F. Delaglio, S. Grzesiek, G. W. Vuister, G. Zhu, J. Pfeiffer, and A. Bax, NMRPipe—A multidimensional processing system based on UNIX pipes, *J. Biomol. NMR* **4,** 277–293 (1995).
14. V. Sklenar, M. Piotto, R. Leppik, and V. Saudek, Gradient-tailored water suppression for $^1H-^{15}N$ HSQC experiments optimized to retain full sensitivity, *J. Magn. Reson. A* **102,** 241–245 (1993).